Impact of Cu(II) Binding on Structures and Dynamics of Aβ₄₂ Monomer and Dimer: Molecular Dynamics Study
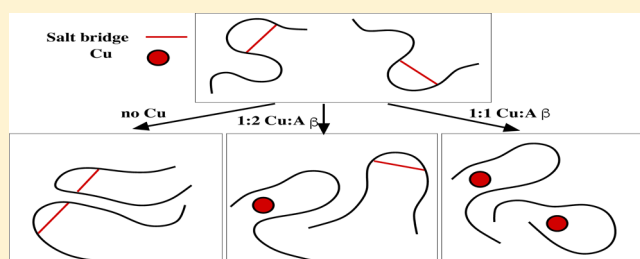
Pham Dinh Quoc Huy,[†,‡] Quan Van Vuong,[‡,§] Giovanni La Penna,*[∥,⊥] Peter Faller,[#] and Mai Suan Li*[†]

[†]Institute of Physics, Polish Academy of Sciences, Al. Lotnikow 32/46, 02-668 Warsaw, Poland

[‡]Institute for Computational Science and Technology, Quang Trung Software City, Tan Chanh Hiep Ward, District 12, Ho Chi Minh City, Vietnam

[§]Department of Chemistry, Nagoya University, Nagoya 464-8602, Japan

[∥]National Research Council of Italy CNR, Institute for Chemistry of Organometallic Compounds ICCOM, 50019 Florence, Italy

[⊥]Italian Institute for Nuclear Physics INFN, Section of Roma-Tor Vergata, 50019 Florence, Italy

[#]Biometals and Biological Chemistry, Institute of Chemistry, University of Strasbourg, 4 rue B. Pascal, 67081 Strasbourg, France

S *Supporting Information*

ABSTRACT: The classical force field, which is compatible with the Amber force field 99SB, has been obtained for the interaction of Cu(II) with monomer and dimers of amyloid-β peptides using the coordination where Cu(II) is bound to His6, His13 (or His14), and Asp1 with distorted planar geometry. The newly developed force field and molecular dynamics simulation were employed to study the impact of Cu(II) binding on structures and dynamics of Aβ₄₂ monomer and dimers. It was shown that in the presence of Cu(II) the β content of monomer is reduced substantially compared with

the wild-type Aβ₄₂ suggesting that, in accord with experiments, metal ions facilitate formation of amorphous aggregates rather than amyloid fibrils with cross-β structures. In addition, one possible mechanism for amorphous assembly is that the Asp23−Lys28 salt bridge, which plays a crucial role in β sheet formation, becomes more flexible upon copper ion binding to the Aβ N-terminus. The simulation of dimers was conducted with the Cu(II)/Aβ stoichiometric ratios of 1:1 and 1:2. For the 1:1 ratio Cu(II) delays the Aβ dimerization process as observed in a number of experiments. The mechanism underlying this phenomenon is associated with slow formation of interchain salt bridges in dimer as well as with decreased hydrophobicity of monomer upon Cu-binding.

KEYWORDS: *Amyloid-β aggregation, copper ions, copper binding to amyloid-β, Alzheimer's disease, amyloid-β peptide, metal ions, Aβ−Cu interaction, protein aggregation, fibril formation*

Alzheimer's disease (AD) is one of the most common age-related neurodegenerative diseases causing cognition decline.[1] Pathologically, the loss of brain's synapses and the presence of progressive extracellular amyloid-β (Aβ) plaques[2] or intracellular neurofibrillary tangles (NFTs)[3] are considered as hallmarks associated with AD. Recently accumulated genetic and pathological evidence strongly support the amyloid cascade hypothesis that the aggregation of Aβ peptides is correlated with the death of neuronal cells.[4,5]

Aβ peptides, produced by proteolytic cleavage of amyloid precursor protein (APP) by β- and α-secretases, mostly consist of 40 (Aβ₄₀) and 42 (Aβ₄₂) residues. They are soluble in a water environment under certain conditions, but at physiological conditions they can form oligomers and aggregate into fibrils and plaques. In the past, amyloid plaques were claimed as toxic species to brain cells.[6,7] However, recent studies suggested that smaller soluble Aβ oligomeric agents are more toxic to neurons rather than mature amyloid fibrils.[2,5,8]

In amyloid plaque areas of the AD-affected brain, a remarkably high concentration of transition metal ions Cu, Zn, and Fe, released by neuronal excitation, has been found.[9−11] The role of metal ions in AD progression attracts considerable attention because their binding to Aβ can catalyze oxidation reactions such as ROS production or Fenton-like reactions causing oxidative stress and cell damage.[11−13]

Many experimental data obtained *in vitro* report significant effects of Cu in the early events of Aβ aggregation. Here we summarize the most evident effects:

1. The coordination of Cu^{2+} to Aβ is in region 1−16, that is, the N-terminus. Though the Cu-binding is dynamic, the major ligand atoms are N and O of Asp1 and Nδ or Nε belonging to two histidine side chains, one of His6 and
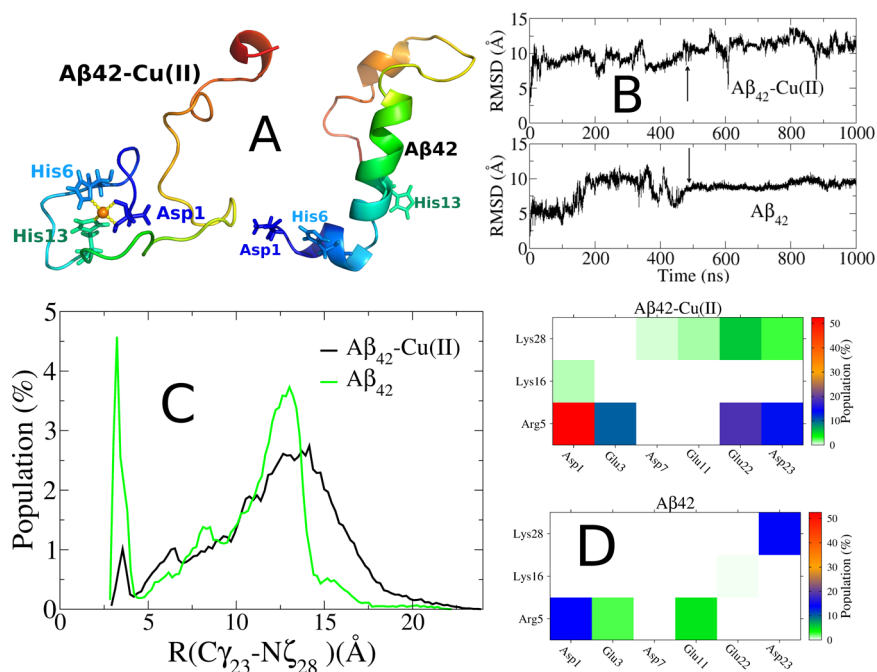
Figure 1. (A) Starting configurations for MD simulations of $A\beta_{42}$ and $A\beta_{42}$−Cu. (B) Time dependence of C_α RMSD for these systems, where the arrow refers to time when they reach quasi-equilibrium. (C) The distribution of the salt bridge distance between atoms $C\gamma_{23}$ and $N\eta_{28}$. (D) Salt bridge contact maps for dimers: black circle refers to SB with population exceeding 10%.

one of either His13 or His14.[14,15] In this study, we focus on the coordination mode (often called component I) that is predominant at neutral pH (compared with the second component, inidicated as II) and is almost exclusively present at slightly acidic pH, the latter conditions relevant for AD and aggregation.

2. The addition of Cu to $A\beta$ in the ratio 1:1 has the effect of delaying the decrease of monomer concentration in the sample compared with pure $A\beta$.[16]

3. The addition of Cu to $A\beta$, independent of the Cu/$A\beta$ ratio, enhances the formation of amorphous aggregates, while $A\beta_{42}$ rapidly forms stable fibrils.[16,17]

In order to possibly prevent the formation of soluble toxic forms of $A\beta_{42}$−Cu complexes, the understanding of the effects of different ratios of Cu on $A\beta$ samples is required. But the understanding of these effects in terms of molecular models is still missing. Quantum mechanical methods, which are accurate in description of bond breaking and forming, are not applicable to study the aggregation of $A\beta$ peptides in complex with metal ions because they are computationally too expensive. The only choice is to use classical molecular dynamics (MD) simulations with reasonable empirical force fields (FFs) describing metal−protein interactions. Intensive MD simulations have been performed for studying $A\beta$ self-assembly without metal ions.[18] The impact of Zn(II) on conformational spaces of $A\beta$ monomers,[19] oligomers[20] and fibrils,[21] has been examined. Miller et al.,[21] for instance, showed that Zn ions promote $A\beta$ aggregation via a population shift of polymorphic states.

Polymorphic states of Cu(II) bound truncated $A\beta_{1-16}$ peptides were characterized by computational simulations.[22] Conformational changes of full-length monomer $A\beta_{42}$ upon Cu(II) binding have been also studied[23,24] by MD simulations. However, the nonbonded model that was adopted to treat Cu(II) by Kozmon and Tvaroska[24] does not allow for describing high binding affinity of Cu(II) as observed via spectroscopies for

the most abundant species at neutral pH.[14,15] Three different $A\beta_{42}$−Cu(II) complexes were described in the harmonic approximation and used in simulations,[23] but those coordinations[25] are not supported as major components by more recent experimental[14,15,26] and theoretical[27,28] works. Thus, the question about the effect of Cu(II) on the structures and dynamics of $A\beta$ monomers remains largely open. Combining solid state NMR and classical MD simulations, it has been shown that Cu(II) does not distort much the structure of $A\beta_{40}$ fibrils when the binding occurs to sites different from those known for the monomer.[29] To our best knowledge, the influence of Cu(II) on the $A\beta$ aggregation kinetics has not been addressed by computer simulations.

In this work, we study the impact of Cu(II) on secondary structures of monomers and the kinetics of dimerization of $A\beta_{42}$ by all-atom MD simulations assuming that Cu(II) is bound to ligands indicated by the most favorable coordination at neutral pH. Therefore, the focus of this study is the Cu coordination involving Asp1, His6, and one of the His13/His14 side chains, assuming other possible coordinations with negligible effects at neutral pH. The first step is to determine force field (FF) parameters comparable to the well-known Amber force field[30,31] for Cu(II)−$A\beta$ interactions in the bonded model. Xu et al.[22] have also developed a set of FF parameters but for the conformer [His6,His13,His14]. Moreover, a tetrahedral geometry was used instead of distorted planar. The FFs were obtained for several coordinations by Parthasarathy et al.,[29] but they are not suitable for our purpose because the dummy atom model, which allows for ions to escape from the binding site at relatively short time scales, has been used.

By the modified Seminario method[32] and the bonded model, we obtained parameters describing the Cu(II)−$A\beta$ bonded model consistent with most of the experimental information for component I.[33] The new FF was implemented in the Amber package to conduct MD simulations for $A\beta_{42}$ monomer and dimers with Cu(II)/$A\beta$ stoichiometric ratios of 1:1 and 1:2. It

Table 1. Structural Parameters[a] for Monomeric Forms

	R_g	SB	HB	SASA	β-sheet	α-helix	turn	coil	$P(CN_3>2)$
$A\beta_{42}$	1.02	0.35	7	31.6	10.0	4.2	19.5	66.3	0.04
$A\beta_{42}$–Cu	1.08	1.07	12	36.0	0.6	1.2	14.3	84.0	0.98

[a]Gyration radius (R_g, nm), number of salt bridges (SB); number of intramolecular hydrogen bonds involving N–H backbone bonds (HB); solvent accessible surface area (SASA, nm^2); probability for ligand preorganization in the "component I" Cu-binding site ($P(CN_3>2)$). β-content, α-helix, turn, and coil are secondary structures measured in %.

was shown that the β-content of monomer is reduced substantially by Cu(II). Because β-rich monomers can serve as precursors for fibril formation,[34] this result is consistent with experiments[16,17] showing that metal ions induce formation of aggregates that are amorphous rather than amyloid fibril. The other mechanism, revealed by MD simulations, for amorphous assembly is that the Asp23–Lys28 salt bridge, which plays a decisive role in stabilizing β-sheet formation, becomes more flexible upon Cu(II)-binding. For the first time, we found evidence that, in agreement with experiments, Cu(II) modulates the dimerization process for $A\beta_{42}$ peptides: the mechanism for interactions between monomers in dimers depends on the extent of Cu-loading. For the Cu(II)/$A\beta$ ratio 1:1, the aggregation process is slowed by Cu ions.

■ RESULTS AND DISCUSSION

Equilibration Time. We have performed 1 μs MD simulation for all systems, both monomeric and dimeric. For monomeric systems, single initial random configurations (see Methods) were used, and the starting configurations are shown in Figure 1A. For dimeric systems, seven different initial conditions were used (see below and SI for details), except for the $A\beta_{42}$–Cu–$A\beta_{42}$ (six initial conditions). Recent results of microsecond-long trajectories show that even when MD simulations have been longer than in the past, convergence issues were not solved for disordered proteins in this time scale.[35] The analysis of several autocorrelation functions for structural properties (like gyration radius, R_g, and number of interchain contacts, N_{ICC}) performed for the dimeric systems simulated in this work (see SI) shows that the expected long-time behavior is not displayed. Indeed, the formation of dimers is faster than the change of shape of each monomer. Therefore, as reported in the literature for simpler molecular systems, the equilibration time can be achieved only using many samples of approaching monomers.[36] This task is far beyond the goals of our work, and it introduces the requirement of modeling also different types of Cu-binding in dynamic exchange. Since, for this system size, we can deal only with a bunch of initial configurations (see below), we limit our analysis to the most evident differences between the studied species.

We therefore define a quasi-equilibration time τ_{eq} as the time beyond which the root-mean square deviation[37] (RMSD) from the initial structure fluctuates around a stable value, rather than addressing a full equilibration of the intricate disordered systems. For monomers (both $A\beta_{42}$ and $A\beta_{42}$–Cu), $\tau_{eq} \simeq 490$ ns (Figure 1). Snapshots collected every 10 ps in the last 510 ns of trajectory were used to estimate relevant quantities in quasi-equilibrium. As for dimers, except for the $A\beta_{42}$–Cu–$A\beta_{42}$ system, five MD trajectories were performed starting from different random seeds (generating different initial velocity fields) and two MD trajectories were performed with different starting atomic configurations. For $A\beta_{42}$–Cu–$A\beta_{42}$, only 1 MD trajectory was changed in atomic coordinates. Insets in Figures S2–S5 display cartoons of the selected initial configurations. As

evident from the time dependence of RMSD and N_{ICC} (see SI), the studied systems reach the above-defined quasi-equilibrium at different time scales (Figure S7 and Table S1 in SI).

Impact of Cu(II) on Monomer $A\beta_{42}$. *Gyration Radius (R_g).* A comparison between some structural parameters obtained in the absence and presence of Cu bound to monomeric $A\beta$ is reported in Table 1. The simulation of $A\beta_{42}$ shows that the peptide adopts, on average, a compact structure. The gyration radius is only slightly larger than that in experiments: 1.01 ± 0.06 nm compared with the experimental value of 0.9 ± 0.1 nm.[38]

The simulation of $A\beta_{42}$–Cu shows that the binding of Cu does not significantly increase the size of the molecule within the simulated time (microsecond) having $R_g = 1.08 \pm 0.08$ nm. A slight increase in the gyration radius is consistent with the increased solvent accessible surface area (SASA) upon Cu binding (Table 1). Recent results obtained by ion mobility mass spectrometry for $A\beta_{40}$,[39] show that the addition of Cu to $A\beta_{40}$ produces monomeric ions with smaller size than in the absence of Cu. Our calculations, when performed for the $A\beta_{40}$ monomer, provides $R_g = 1.13 \pm 0.36$ nm for $A\beta_{40}$–Cu and $R_g = 1.19 \pm 0.22$ nm for $A\beta_{40}$, respectively. Therefore, the addition of Cu to $A\beta_{40}$ has the opposite effect compared with the addition of Cu to $A\beta_{42}$. Interestingly, the different behavior of $A\beta_{42}$ and $A\beta_{40}$ with respect to the change in monomer size with Cu addition is reflected in the behavior of other structural properties (see below).

Salt Bridge Network. We performed a careful inspection of salt bridges (SB) formation during simulation. Because $A\beta_{42}$ has three positively charged and six negatively charged residues, we have 18 possible SBs. The population of Asp23–Lys28 SB obtained in the last 510 ns of MD simulations is shown in Figure 1C, while Figure 1D depicts the full SB contact map.

Lys28 predominantly forms SB with Asp23 (Figure 1D) but not with Glu22. Lys16 forms a salt bridge with Asp23 for a very short time at the end of simulation, while it is more often in contact with Glu11. Arg5 mainly interacts with other charged residues within the 1–16 region, particularly with Asp1. It has a very weak interaction with Asp23 from the C-terminus.

This behavior can be summarized as follows. The structure of $A\beta_{42}$ is compact almost as it is found in experiments for the transient monomeric state. The number of intramolecular hydrogen bonds seals the compact structures to a larger extent compared with salt bridges. This latter feature is not present in the structure packed into the fibril, where the intramolecular hydrogen-bond network is entirely displaced toward the close partner in the fibril and the salt bridge Asp23–Lys28 is almost the unique intramolecular force contributing to the monomer compaction.

The most significant changes compared with the non-Cu case deal with the network of electrostatic interactions. The Asp23–Lys28 salt bridge is less likely than with no Cu bound to $A\beta$, but on average, about one more salt bridge is formed in total (Figure 1D). With Cu, the probability of a salt bridge Lys28–Asp23 is as
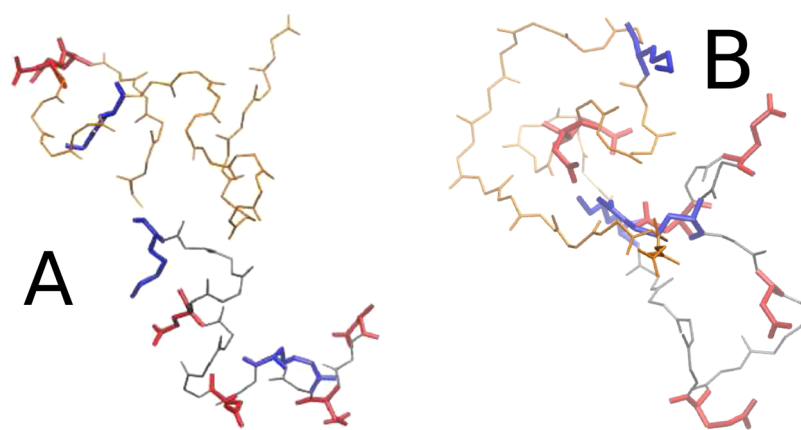
Figure 2. Comparison between the structures with maximal SB for $A\beta_{42}$ monomer (A) and $A\beta_{42}$−Cu monomer (B). One has SB = 3 (A) and SB = 4 (B). The 1−16 region backbone is in gray, the 17−42 is in orange; atoms belonging to Asp/Glu residues are in red, those of Lys/Arg are in blue.

likely as that with Asp7, this latter bridging the 1−16 N-terminal region to the turn region. Lys16 forms salt bridges with Asp1 and Asp23 in a short time range with both again forming a long-range bridge connecting the N-terminal region 1−16 with the region involved in the turn. Arg5 forms a persistent salt bridge with Asp1 but a second salt bridge (for 1/4 of the simulation) with Asp23. Therefore, both Arg5 and Lys16 interact with Asp23, diverting Asp23 away from Lys28. This latter becomes available to interact with other partners.

It is interesting to notice that this network of electrostatic interactions affects the extent of intramolecular hydrogen bonds and the SASA. The presence of Cu bound to $A\beta$ hinders the increase of intramolecular backbone hydrogen bonds (that is kept constantly smaller in $A\beta$−Cu than without Cu). The increase of about 10% in the SASA (Table 1) indicates a larger propensity of the molecule to be hydrated once Cu is bound to the N-terminus.

Interestingly, despite the different behavior in terms of R_g, as for the SB network, simulations of $A\beta_{40}$ monomer in the presence and absence of Cu provide the same picture of $A\beta_{42}$. In particular, when Cu is added to $A\beta_{40}$ the Asp23−Lys28 SB is destabilized. As a difference compared with $A\beta_{42}$−Cu, the two oppositely charged groups in $A\beta_{40}$−Cu are still kept, with a larger chance, within distances in the range of 5−10 Å (data not shown here), consistent with a change in SB structure together with a simulated average smaller size for $A\beta_{40}$−Cu.

Cu Reduces Hydrophobicity of $A\beta_{42}$ Slowing Aggregation for Stoichiometric Ratios 1:1. Upon Cu binding, SASA of monomer increases from 31.6 to 36 nm² (Table 1) implying reduced hydrophobicity of $A\beta_{42}$. This result may be also corroborated by a more precise argument calculating the solvation free energy, $G_{\text{solvation}}$. In the molecular mechanics Poisson−Boltzmann surface area (MM-PBSA) method,[40] $G_{\text{solvation}}$ is approximated as the sum of electrostatic and nonpolar contributions, $G_{\text{solvation}} = G_{\text{PB}} + G_{\text{sur}}$. Here G_{PB} derived from the electrostatic potential between solute and solvent was obtained using the continuum solvent approximation.[41] Using grid spacing 0.5 Å, the PBSA package in Ambertools was implemented for numerical solution of the corresponding linear Poisson−Boltzmann equation. The nonpolar solvation term, G_{sur}, approximated as linearly dependent on SASA is[42] $G_{\text{sur}} = \gamma\text{SASA} + \beta$, where $\gamma = 0.00542$ kcal/(mol·Å²) and $\beta = -1.008$ kcal/mol. Using snapshots sampled in quasi-equilibrium, we obtained $G_{\text{solvation}} = -667.7$ and -674.4 kcal/mol for $A\beta_{42}$ and $A\beta_{42}$−Cu, respectively. Reduction of the solvation free energy

implies that upon Cu binding $A\beta_{42}$ monomer becomes less hydrophobic leading to delay in aggregation[43,44] as observed in experiments.[16] Note that this conclusion is valid for the Cu/$A\beta$ ratio of 1:1 when one Cu ion is bound to one amyloid-β peptide.

Cu Binding Increases Flexibility of Asp23−Lys28 Salt Bridge Promoting Amorphous Aggregation. It is well-known that the dynamics of this salt bridge plays a central role in formation of fibril with cross-β structure.[18,45] The constraint of a lactam bridge connecting residues 23 and 28 substantially suppresses the lag phase prior to $A\beta_{40}$ nucleation.[46] This observation has been also confirmed by molecular simulations.[47−49] Upon Cu binding, the peak of distribution of the salt bridge distance moves toward much larger distance (Figure 1C) implying its enhanced flexibility. The Asp23−Lys28 population is reduced from 13.8% to 2.8% (Figure 1D), while the mean distance between $C\gamma_{23}$ and $N\zeta_{28}$ increases from 0.97 to 1.12 nm. Because the constraint of the Asp23−Lys28 salt bridge promotes the amyloid fibril formation, our data are in agreement with those experiments demonstrating that Cu ions facilitate amorphous aggregation.

The Change in the Network of Electrostatic Interactions between Region 1−16 and Region 17−28 Swells the Peptide. In Figure 2, the structures with maximal number of salt bridges (SB) are displayed for $A\beta_{42}$ (panel A) and $A\beta_{42}$−Cu (panel B). It can be noticed that when no Cu is bound to $A\beta$, the 1−16 region forms the maximal number of contacts within the region, while no electrostatic interactions are formed between the N- (1−16) and C- (17−42) terminal regions. This allows an easy interaction between Glu22−Asp23 and Lys28 within a well-separated C-terminus. On the other hand, when Cu is present, the two regions are more interconnected, especially by Arg5, which is able to interact with more than one partner at the same time. In this condition, Lys28 is left free to interact, eventually with Asp/Glu partners in other monomers.

With Cu, the Two Subunits (1−16 and 17−42) Are Interconnected by Several Salt Bridges, while with No Cu the Two Subunits Are More Independent. The simulation of $A\beta_{42}$ in the monomeric form allows an approximate measurement of the probability for candidate Cu ligand atoms to be collected in the same region of space. We focus on three sets of ligand atoms: $N\delta$ and $N\epsilon$ of His 6 (set 1), N and O of Asp1 (set 2), and $N\delta$ and $N\epsilon$ of His 13 and 14 (set 3). The CN_3 value (with $d_0 = 0.3$ nm, see Methods) based on the three sets of atoms is used as a measure of the ligand preorganization to bind Cu in the "component I" topology. In the Cu-bound monomer,
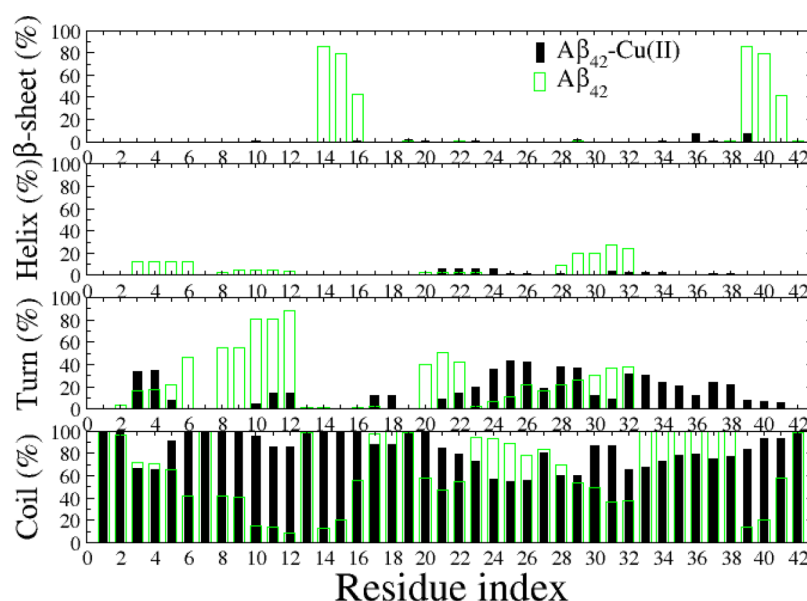
Figure 3. Average per-residue distributions of secondary structures of monomers Aβ_{42} and Aβ_{42}–Cu.

Table 2. Average Structural Parameters for Dimers[a]

	R_g	SASA	β-sheet	α-helix	turn	coil	$P(CN_3>2)$ (%)	
							mono A	mono B
$(A\beta_{42})_2$	1.39	57.6	8.0	11.0	24.0	57.0	5.9	0.2
$(A\beta_{42}-Cu)_2$	1.39	60.4	9.1	2.3	15.4	73.2	97.6	98.2
$(A\beta_{42}-Cu) + A\beta_{42}$	1.38	58.9	8.7	5.3	17.5	68.5	98.5	0.6
$A\beta_{42}-Cu-A\beta_{42}$	1.32	57.7	7.3	3.0	17.2	72.5	0.0	99.1

[a]R_g (nm), SASA (nm^2), secondary structure percentages, and population $P(CN_3>2)$ for four dimeric systems.

the CN$_3$ is 5.5 ± 0.5, as expected by the presence of Nδ(His 6), both N and O of Asp1, and Nϵ of His13 in the Cu-coordination sphere. This arrangement counts 3 × 2 pairs within the given distance of 0.3 nm.

In the case of Cu-free monomer, the probability of CN$_3$ > 2 is small (0.04, see Table 1), three atoms being within the coordination sphere in about 40 configurations over 1000 collected. As a term of comparison, the probability of CN$_3$ > 2 is zero when the second set is replaced with O atoms of carboxylic groups (any Asp and Glu residue in the sequence), thus showing that the N-terminus has a significant probability to approach His6 side chain, together with one of the His side chains in the 13−14 segment. As expected, in the presence of Cu(II), the probability of CN$_3$ > 2 is nearly 1 (Table 1).

Cu(II) Reduces β-Content. The high β-content occurring at residues 19−23 (Figure 3) is consistent with Rosenman et al.[50] who observed high β-population in residues 16−23 using the OPLS-AA/L force field with explicit water model TIP3P. All-atom simulations with Amber ff99SB force field and TIP4P-Ew water show that region 16−21 is rich in β-structure.[51] The C-terminus is rich in β-propensity (Figure 3) at residues 39−41, consistent with other theoretical studies showing that the β-structure mainly occurs at 38−41[52] and 37−40.[53]

The overall β-content of Aβ_{42} is about 10% (Table 1), which falls in the range of experimental estimates.[18] In the presence of Cu(II), the system becomes poor in well-defined secondary motifs. The β-structure drops to 0.6%. This result qualitatively agrees with the experimental finding that copper ions facilitate formation of amorphous aggregate rather than amyloid fiber.

In accord with other theoretical works,[54−57] the α-content of Aβ_{42} is low (Figure 3 and Table 1) and lower than the result reported by Yang and Teplow.[58] Upon Cu(II) binding, the helix ordering becomes even weaker as α-content drops from 4.2% to 1.2%. The random coil (coil + turn) of Aβ_{42} is 85.8% (Table 1) falling into the range of other simulation estimates.[52,54,55,58,59] The increase in random coil in the presence of Cu(II) further supports the experimental fact that metal ions promote amorphous aggregation. The coil content at Asp1 coordinated to Cu(II) remains intact, but it increases substantially at histidine positions 6, 13, and 14 (Figure 3).

Dimers. We have studied four systems: dimer $(A\beta_{42})_2$ without Cu, dimer $(A\beta_{42}-Cu)_2$, where each chain is bound to Cu, $A\beta_{42} + (A\beta_{42}-Cu)$, where Cu is complexed with one chain, and $A\beta_{42}-Cu-A\beta_{42}$, where Cu is bound to two chains in component I.

Gyration Radius. The impact of Cu on R_g of dimers is minor (Table 2). The coordination of Cu(II) to both chains reduces the gyration radius to a greater extent compared with other systems, leaving SASA almost the same as in the free Cu case. As seen below, the increase in SASA is rather associated with the salt bridge network than R_g. The enhanced compactness of dimers upon Cu-binding is in line with the experimental observation on amorphous aggregation and with the recent results obtained by ion mobility mass spectrometry for Aβ_{40}.[39]

Secondary Structure. Dimer without Cu: $(A\beta_{42})_2$. We first compare our results obtained for secondary structures of Cu-free dimer $(A\beta_{42})_2$ with experiments and previous theoretical works. NMR and CD studies of low molecular weight Aβ dimers and multimers as large as heptamers in equilibrium give 15−
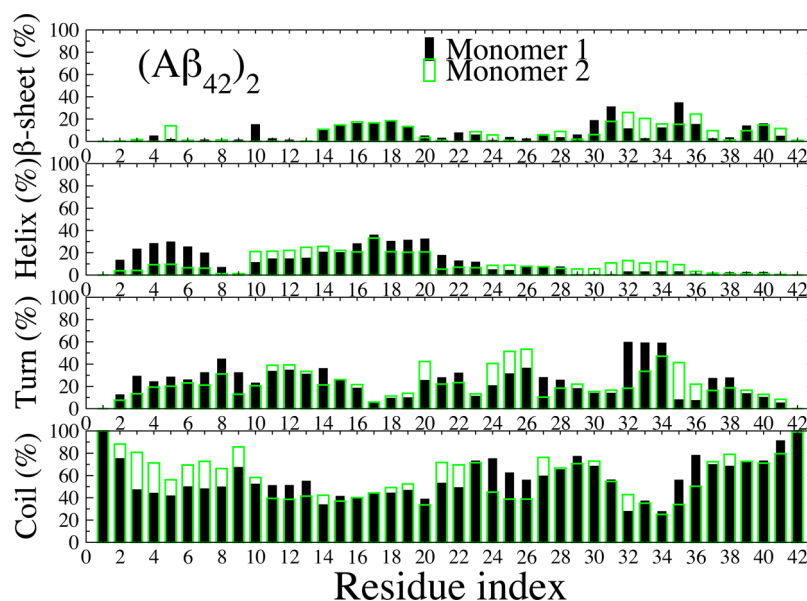
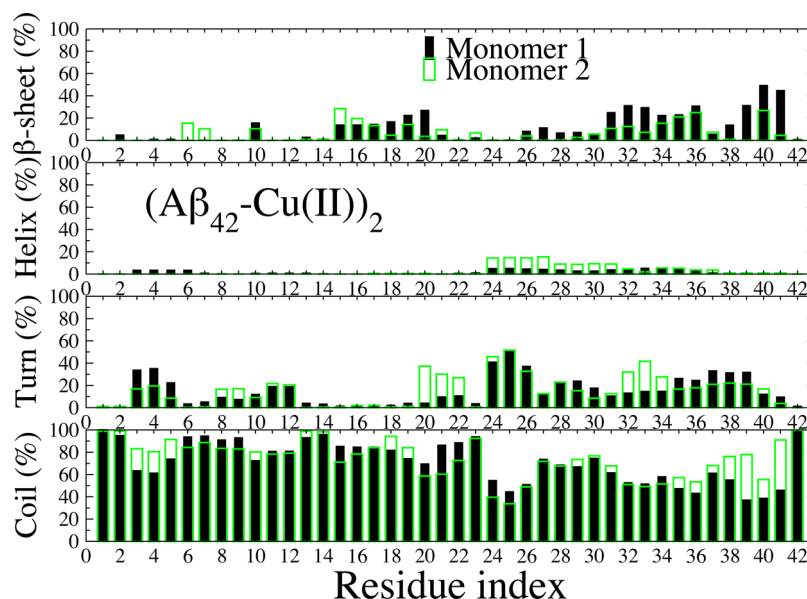**Figure 4.** Average secondary structure of dimer without Cu.

Figure 5. Average secondary structure of dimer $(A\beta_{42}-Cu)_2$ (Cu/Aβ ratio 1:1).

25% β-strand, and <10% α-helix.[60−62] Our estimations of $\beta \approx$ 13% and α = 6.5% (Table 2) are roughly consistent with these experiments. Much higher β-content was obtained using the OPEP coarse grained model (30%)[55] and DMD simulation based on the four-bead model (20%).[63] However, DMD-MD multiscale approach gives a percentage of 6% β-strand,[64] which is close to 8% provided by extensive all-atom REMD simulations with OPLS force field in explicit solvent.[65] Zhang et al.[65] have also shown that, in agreement with our result (Table 2), Aβ_{42} dimer predominantly populates coil/turn (80.4%). Thus, upon dimerization, the β-content slightly increases (compare Tables 1 and 2) supporting the strong propensity of Aβ_{42} to self-assembly into fibrils.

Impact of Cu(II) on Secondary Structures of Dimers. The presence of Cu does not influence much the mean value of β-structure of $(A\beta_{42}-Cu)_2$ and Aβ_{42}−Cu + Aβ_{42}, remaining about 12% (Table 2). Per-residue distributions also show that the

fibril-prone regions at both termini of these dimers are more populated by β-strands than other regions (Figures 4, 5, and 6). The situation is very different for Aβ_{42}−Cu−Aβ_{42}, where the β-content is notably reduced from 12.9% to 7.3% upon Cu-binding implying the increased propensity to amorphous self-assembly rather than to amyloid fibers. This conclusion is further supported by very poor β-structure at the C-terminus (Figure 7). The high coil content of all Cu-bound dimers relative to the Cu-free $(A\beta_{42})_2$ (Table 2) agrees with the experimental finding on Cu-induced amorphous aggregation. As expected, α-helix is reduced in the presence of Cu ions, particularly for dimer with the 1:1 stoichiometry (Table 2 and Figures 4−7).

Salt-Bridge Networks. Dimer without Cu: $(A\beta_{42})_2$. Contrary to the monomer case, where SBs between 1−16 and 17−42 regions did not appear during MD simulations (Figure 3), intrachain SBs between N and C termini were sampled in dimer
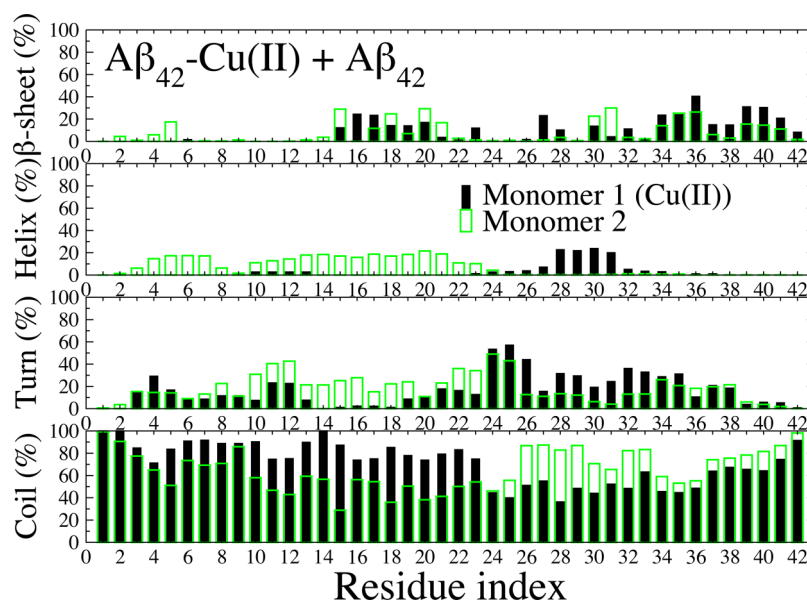
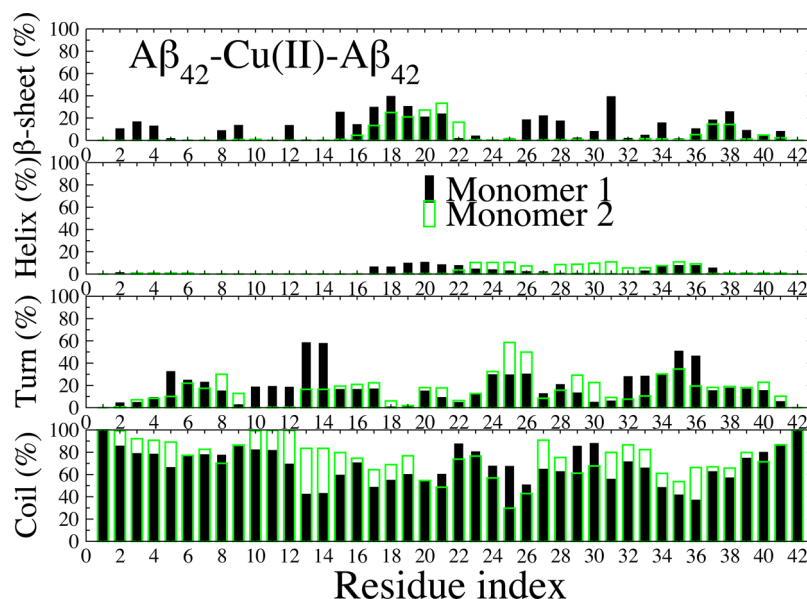**Figure 6.** Average secondary structure of dimer $(A\beta_{42}-Cu) + A\beta_{42}$ (Cu/Aβ ratio 1:2).

Figure 7. Secondary structures of dimer $A\beta_{42}-Cu-A\beta_{42}$ with Cu/Aβ ratio 1:2.

$(A\beta_{42})_2$ (Figure 8). Arg5A (Arg5A means Arg5 from chain A) forms SB with Asp23A, while Lys28A interacts with Glu11A. Because population of these contacts is rather low (below 20%) and similar SBs were not sampled for monomer B, the electrostatic interaction between two termini within each monomer remains weak with no Cu.

The salt bridges present in $A\beta_{42}$ dimers involve almost separately 1−16 and 17−42 regions. Lys28 of monomer A forms a salt bridge with the Glu22 from monomer B with the population much higher than with Asp7B, while Arg5 of monomer A strongly interacts with Asp1-x-Glu11 segment in monomer B (Figure 8). The electrostatic interaction of Lys16A with Asp1B and Glu11B is much stronger than that with Glu22B. Arg5 of monomer B interacts with Asp1 and Glu3 of monomer A.

Overall, only a few salt bridges with low population are formed between regions 1−16 and 17−42, thus showing that

when dimers are formed the cross-talk between monomers hinders the cross-talk between different regions. Moreover, this in-register electrostatic interaction favors a parallel orientation of monomer sequences. Accordingly, very rare salt bridges between the N-terminus of monomer A and C-terminus of monomer B were observed.

Dimer with Cu/Aβ_{42} Ratio 1:1 ($(A\beta_{42}-Cu(II))_2$). In the presence of Cu, the number of populated SBs is reduced from 36 to 28 (Figure 8). Among them, the decrease in interchain SBs is more pronounced with reduction of 17 to 10 SBs. The reduction of SBs due to Cu becomes even more drastic taking into account only contacts with population exceeding 10% because one has 13 SBs in the absence of Cu and only 6 SBs with it. Cu breaks some SBs but promotes formation of the new ones such as Lys28B with Asp7A and Glu11A and Lys16B with Asp23A. Because fibril structures are expected to be locked by stable interchain contacts, the reduction of SBs is in line with the
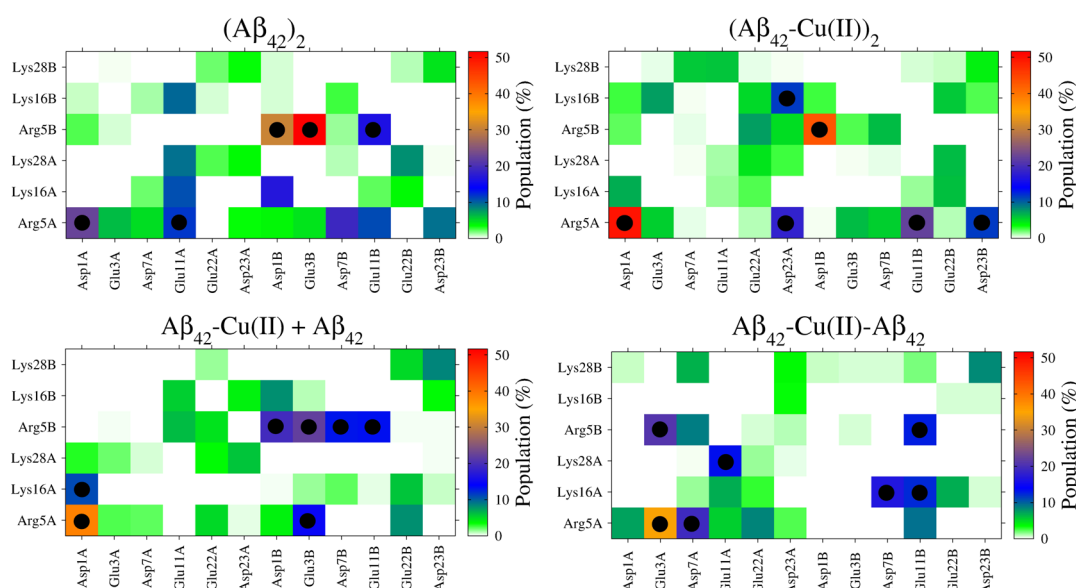
Figure 8. Salt bridge contact maps for dimers. Black circle refers to SB with population exceeding 10%.
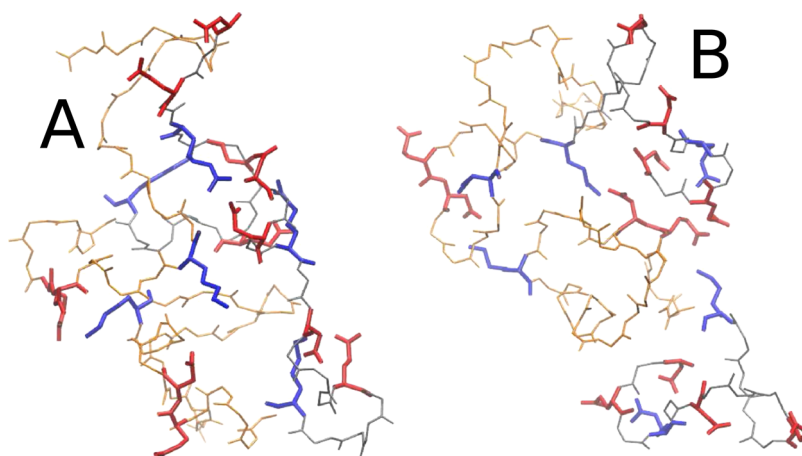

Figure 9. Comparison between the structures with maximal SB for $(A\beta_{42})_2$ dimers (A) and $(A\beta_{42}-Cu)_2$ dimers (B). The number of salt bridges SB = 9 (A) and SB = 8 (B). Color scheme is as in Figure 2.

experimental observation that copper ions promote amorphous aggregation.

The maximal SB structures for $(A\beta_{42})_2$ and $(A\beta_{42}-Cu(II))_2$ are compared in Figure 9, panels A and B, respectively. It can be noticed that the in-register interactions present with no Cu are broken with Cu. In this latter case, most of the charged groups are exposed to water. Particularly noticeable is the release toward the solvent of two almost independent 1−16 regions.

Dimers with Cu/$A\beta_{42}$ Ratio 1:2 (($A\beta_{42}-Cu(II)$) + $A\beta_{42}$ and $A\beta_{42}-Cu(II)-A\beta_{42}$). As in the $(A\beta_{42}-Cu(II))_2$ case, the total number of SBs decreases upon Cu-binding with 31 and 32 SBs for $(A\beta_{42}-Cu(II))$ + $A\beta_{42}$ and $A\beta_{42}-Cu(II)-A\beta_{42}$, respectively (Figure 8). Taking into account only SBs with population above 10% the corresponding numbers reduced to 8 and 10, which are lower than 13 of the dimer without Cu. In $(A\beta_{42}-Cu(II))$ + $A\beta_{42}$, there is no cross talk between 1−16 and 17−42 regions of each monomer. This is in contrast with $A\beta_{42}-Cu(II)-A\beta_{42}$ where the connection between these regions of monomer A exists due to SB Lys28A−Glu11A and Arg5A−Glu22A, while the cross talk is absent in monomer B. Due to tight Cu binding to both chains, the attractive electrostatic interaction between

two monomers of $A\beta_{42}-Cu(II)-A\beta_{42}$ is stronger than that of $(A\beta_{42}-Cu(II))$ + $A\beta_{42}$. This is evident from the fact that the former system has four highly populated interchain SBs against three of the latter (Figure 8).

The importance of SBs on the rate of $A\beta$ nucleation has been discussed in the literature, combining mutation experiments and computational models.[66] In particular, electrostatic interactions have been addressed in stabilizing oligomeric protofibrils assembled as in the structure of amyloid fibril determined by ssNMR.[67] In the MD simulations of $A\beta(9-40)$ peptides assembled in protofibrillar oligomers and fibrils, the array of a one-dimensional ionic crystals is put in evidence at room temperature.[68] The exchange between Asp23 and Glu22 in the ionic interaction with Lys28 is found as an early event in the protofibril melting.

Several computational studies performed by approaching protofibrillar oligomers to membranes showed that electrostatic interactions between charged side chains of $A\beta(9-40)$ and charges of the phospholipid headgroups play an important role,[69] up to triggering a significant thinning of membrane

bilayer.[70] The latter event was associated with the experimentally observed cytotoxic effects of Aβ oligomers.

As for the ligand preorganization to Cu-binding in the component I topology, the probability of preorganized coordination in one of the monomers is quite large when Cu is not present ($P(CN_3 > 2) = 9\%$, Table 2). This explains the rapid binding of one Cu to Aβ(1−42) when no Cu is yet loaded. When at least one monomer in the dimer is loaded with Cu, the probability becomes zero. This observation shows that when the 1:2 Cu/Aβ dimer is formed, a large reorganization of the peptide is required to host a second Cu ion in the same dimer. Alternative reactions, like the formation of larger oligomers, may compete with further Cu binding. This result is consistent with experiments,[16] since the Cu binding is fast and stoichiometric when Cu is added at low ratio to Aβ (0.25:1), while it is very slow when the ratio is 1:1. Even though the final ratio in Aβ_{42} aggregated forms is 1.4:1, the binding of Cu to Aβ_{42} is hindered when a small amount of Aβ_{42} is in complex with Cu.

Impact of Cu Ions on Aggregation Rate: Evidence from SB Network. As seen above, for the system with 1:1 ratio the delay in aggregation may be inferred from reduced hydrophobicity of monomer in the presence of Cu. Here we try to understand this and other systems using data collected for dimers.

The impact of Cu(II) on aggregation rates may be understood monitoring the time dependence of the number of interchain contacts N_{ICC} (Figures S2−S5 in SI). Because we study the process of oligomerization, the MD trajectory that started from the ordered conformation (trajectory 1′ for Aβ_{42}−Cu−Aβ_{42} and 1″ for three other dimers) should be excluded. In quasi-equilibrium, within error bars, the mean numbers of interchain contacts N_{ICC} are not distinguishable for Cu-free and Cu-bound dimers (Table 3). This also holds for interchain HBs and SBs. Thus, based on averaged quantities, one cannot gain insights on influence of Cu(II) on Aβ_{42} dimerization.

Table 3. Average Values of Interchain Contacts (N_{ICC}), HBs, and SBs[a]

system	interchain SB	interchain HB	interchain contact
(Aβ_{42})$_2$	0.7 ± 0.8	2.1 ± 1.5	26.7 ± 3.0
(Aβ_{42}−Cu)$_2$	1.1 ± 0.5	2.9 ± 1.4	34.2 ± 10.2
(Aβ_{42}−Cu) + Aβ_{42}	0.7 ± 0.8	2.6 ± 0.8	35.0 ± 6.8
Aβ_{42}−Cu−Aβ_{42}	1.1 ± 1.0	2.3 ± 1.7	34.5 ± 9.1

[a]Trajectrories that started from fibril-like conformations were not taken into account.

On the other hand, 3 and 7 interchain SBs have population exceeding 10% for (Aβ_{42}−Cu)$_2$ and (Aβ_{42})$_2$, respectively (Figure 8), implying that interchain SB formation in (Aβ_{42}−Cu)$_2$ is slower than in (Aβ_{42})$_2$. Because the SB locking is important for protein hydrophobic collapse,[71] which is crucial for self-assembly, our result suggests that, consistent with experiments, amorphous aggregation is slowed for the stoichiometric ratio 1:1.

The effect of Cu-binding on interchain SB formation in (Aβ_{42}−Cu) + Aβ_{42} and Aβ_{42}−Cu−Aβ_{42} dimers is not as evident as in the (Aβ_{42}−Cu)$_2$ case (Figure 8). For both systems, one has four interchain SBs with population exceeding 10%. Thus, the question of influence of Cu(II) on Aβ oligomerization rate for Cu(II)/Aβ ratio 1:2 requires further investigation.

Free Energy Landscapes. The FES of dimer without Cu is characterized by four major basins with representative structures shown in Figure 10. As expected, the first two dominant
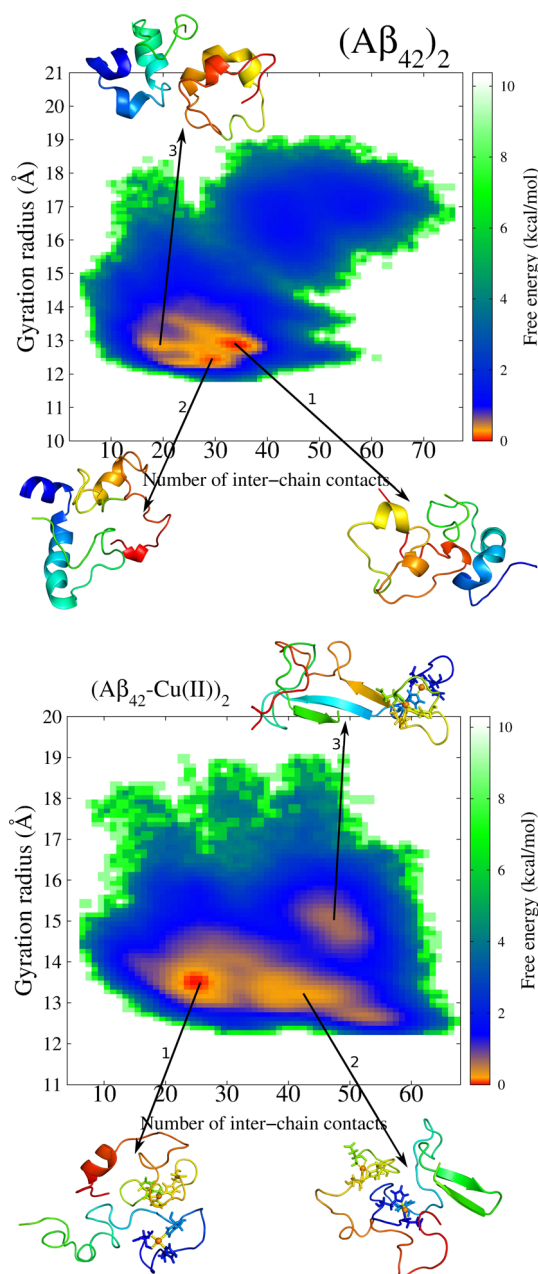

Figure 10. Free energy surfaces (FES) of dimers (Aβ_{42})$_2$ and (Aβ_{42}−Cu)$_2$. Results were obtained with the whole trajectories. Structures representative of basins containing local free energy minima are displayed.

structures S1 and S2 have β-content close to its mean value of ∼13% (Tables 2 and 4). These structures have relatively high α-helix of 14.3%. The main difference between S1 and S2 is that S1 has much more intrachain HBs than S2 and S1 is more compact with smaller gyration radius. Structures S3 and S4, which are less populated compared with S1 and S2, have high β-content of 28.6% but almost no helix. Their ordering is mainly maintained by interchain contacts and hydrogen bonding. S4 has $N_{ICC} = 58$ and the number of interchain HBs of 12 (Tables 4). Highly ordered structures like S3 and S4 presumably can serve as precursors for fibril growth.

In the presence of two Cu ions the FES of (Aβ_{42}−Cu(II))$_2$ becomes narrower along reaction coordinate N_{ICC} (Figure 10) implying that structural fluctuations are less effective than in the

Table 4. Information on Structures Representing Major Basins on Free Energy Surfaces of Dimers (Figures 10 and 11)[a]

	strand	P (%)	ICC	R_g	SB	SB_{AB}	HB	HB_{AB}	SASA	β	α	turn	coil
$(A\beta_{42})_2$	1	2.3	34	12.92	3	0	9	0	55.33	0.0	16.7	22.6	60.7
	2	3.6	28	12.51	1	0	13	2	57.70	2.4	27.4	23.8	46.4
	3	2.0	20	12.86	3	1	10	1	51.67	2.4	17.9	29.8	49.9
$(A\beta_{42}-Cu)_2$	1	2.0	26	13.56	5	1	11	3	61.27	4.8	2.4	26.2	66.6
	2	2.2	42	13.30	1	1	9	5	60.21	14.3	0	15.47	70.2
	3	0.4	46	15.20	2	2	8	3	66.01	26.2	0	16.7	57.1
$(A\beta_{42}-Cu) + A\beta_{42}$	1	4.4	42	13.25	2	1	10	5	59.33	4.8	10.7	16.7	67.8
	2	3.3	27	13.65	1	1	11	3	55.82	20.2	0	21.4	58.4
	3	0.5	49	16.28	1	0	12	4	63.98	20.2	0	16.7	63.1
$A\beta_{42}-Cu-A\beta_{42}$	1	16.2	24	12.27	2	1	9	2	56.12	0.0	0.0	15.5	84.5
	2	4.4	43	12.99	3	0	15	2	55.43	8.3	0.0	20.2	71.5
	3	3.8	57	13.51	2	1	16	6	57.24	14.3	9.5	11.9	64.3
	4	3.5	21	13.52	2	0	14	1	63.68	7.1	4.8	11.9	76.2

[a]Population (P) of snapshots is given in third column. Secondary structures including β, helix, and coil contents are in percentage (%). SB and HB refer to the total number of salt bridges and hydrogen bonds. ICC, SB_{AB}, and HB_{AB} denote interchain contacts, SBs, and HBs, respectively. The mean gyration radius R_g and SASA are measured in Å and nm^2.

Cu-free case. Chains appear more locked into configurations well separated in free energy. In addition all three representative structures S1−S3 are less ordered than S3 and S4 of $(A\beta_{42})_2$ (Table 4). This is in the line with the experimental observation that Cu promotes amorphous aggregation rather than amyloid fibril formation. Among the three structures, S2 has the lowest percentage of secondary motifs, but its SB number is highest suggesting that SB locking is crucial in amorphous self-assembly.

Compared with the Cu-free case, $(A\beta_{42})_2$ (Figure 10), the FES of $(A\beta_{42}-Cu) + A\beta_{42}$ is more compact along both reaction coordinates, while the FES of $A\beta_{42}-Cu-A\beta_{42}$ is more compact along R_g (Figure 11). Therefore, the compactness of peptides in these dimer topologies makes them templates for a fast aggregation into assemblies of small globular particles. These assemblies are expected to be amorphous.

CONCLUSION

We have developed the FF for describing the interaction of Cu(II) with $A\beta$ in the coordination characteristic of component I, that is, the dominant species at neutral pH. It was shown that the presence of Cu(II) reduces the structural ordering of $A\beta_{42}$ monomer, in particular, the β-content suggesting that, in agreement with available experiments, metal ions promote amorphous aggregation. This finding was also supported by enhanced flexibility of Asp23−Lys28 SB upon Cu(II) binding to monomers. Cu-induced reduction of hydrophobicity suggests that $A\beta_{42}$−Cu self-aggregates slower than $A\beta_{42}$.

On the other hand, MD simulations of dimers with and without Cu have also provided evidence that, in agreement with experiments, upon Cu(II) binding the self-assembly is slowed for 1:1 stoichiometry. When a large number of intermolecular salt bridges occur, seeds are more fluid and the aggregation can proceed through an extended hydrophobic collapse. When a reduced number of stable intramolecular salt bridges is formed, like in the 1:1 Cu−$A\beta_{42}$ case, the lifetime of low-order oligomers in water can be significantly enhanced. In this case the prosecution of the hydrophobic collapse is hindered. These soluble dimers are potentially active as homogeneous catalyst, thus being off-pathway in the formation of amorphous aggregates. The latter are likely less active as catalysts.

METHODS

Construction of Force Field Parameters. *Optimization of Cu(II) Coordinations in $A\beta$ Monomer and Dimer.* Initial structures of $A\beta$−Cu(II) complexes, taken from La Penna et al.,[28] were obtained from the Monte Carlo random walks and Car−Parrinello MD simulations. There are eight binding modes for $A\beta$−Cu(II) monomers and eight binding modes for dimers. The study reported in ref 28 does not contain empirical parameters, since it was a study performed with first-principles MD simulations within density-functional theory (DFT) approximation of eight $A\beta_{16}$−Cu(II) monomers and eight $A\beta_{16}$−Cu(II)−$A\beta_{16}$ dimers. The preparation stage of the 16 DFT initial configurations was based on a simplified model for the cation combined with Monte Carlo simulations of the peptide chains.[28,72] None of these parameters were used in the present study. Among the final configurations obtained in the previous study, the most stable structures (see SI for details) were reoptimized by the unrestricted hybrid density functional method (UB3LYP) in SMD implicit solvent[73] available in the Gaussian09 package.[74] The 6-31G(d) and SDD basis sets were employed for C, N, O, and H and Cu, respectively. The optimized structures of $A\beta$−Cu(II) monomer and dimer are shown in Figure 12A,B.

For monomer, Cu bonds to N and O of Asp1, Nδ of His6, and Nϵ of His13 at equatorial positions. There is a contact (4.0 Å) between Cu and Nδ of His14 at the apical position. Similar to monomer, Cu also bonds to these ligands of dimer, but Asp1 and His6 belong to one chain, while His13 and His14 (red) belong to the other one. In addition, the positions of Cu−N(His13) and Cu−N(His14) are exchanged, and the distance between Cu and Nϵ(His13) is only 2.3 Å.

In order to judge the apical close contact as bonded or nonbonded interaction, the bonding energy of apical Cu−N was estimated. The effect of backbone constraining relative position of residues His13 and His14 is removed by constructing a truncated model (Figure 13A) in which His13 and His14 are replaced by imidazole rings. The bonding energy of apical imidazole was calculated as

$$E_{bond} = E_{[Cu+Asp1+His6+2\times imidazole]} - E_{[imidazole]}$$
$$- E_{[Cu+Asp1+His6+imidazole]} \quad (1)$$

The bonding energy of the equatorial imidazole was also calculated in a similar way:

$$E_{bond} = E_{[Cu+Asp1+His6+imidazole]} - E_{[imidazole]} - E_{[Cu+Asp1+His6]} \quad (2)$$

Structures of complexes [Cu + Asp1 + His6 + imidazole] and [Cu + Asp1 + His6] are depicted in Figure 13B,C, respectively. All calculations were performed at the same level as the former optimization in implicit solvent. The calculated bonding energy of
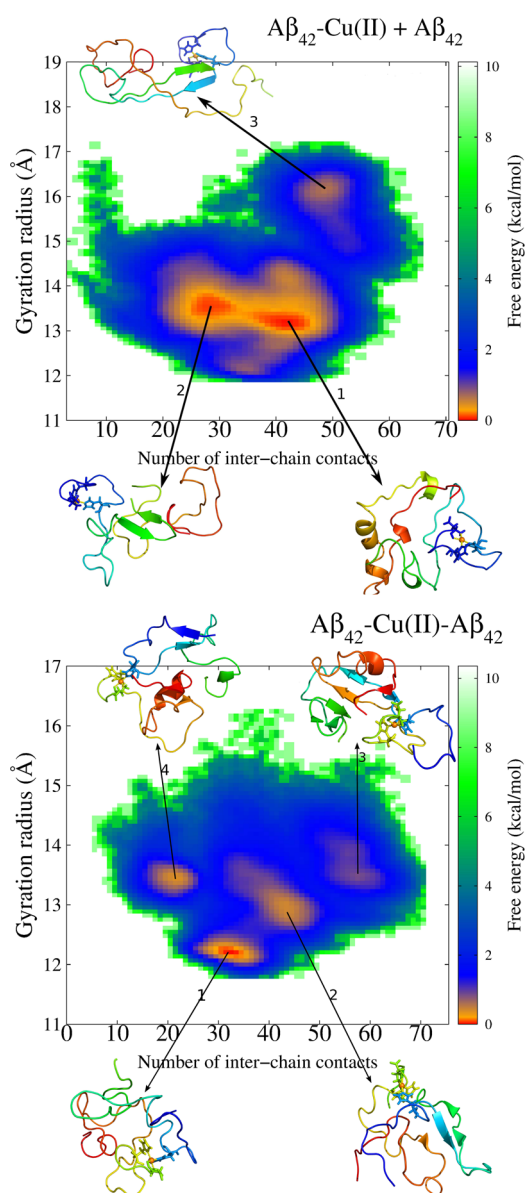
Figure 11. Free energy surfaces (FES) of dimers $(A\beta_{42}-Cu) + A\beta_{42}$ and $A\beta_{42}-Cu-A\beta_{42}$. Results were obtained with the whole trajectories. Structures representative of basins containing local free energy minima are displayed.
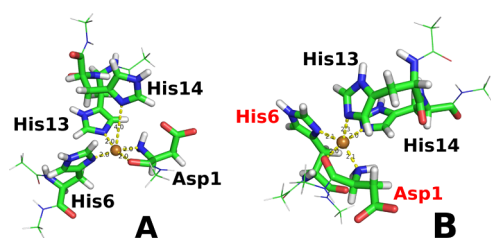

Figure 12. (A) Optimized structure of monomer: copper is displayed as small orange sphere, yellow dotted lines represent bonds between copper and ligands. Bond lengths are in Å. (B) Optimized structure of dimer, where Asp1 and His6 (red) belong to one chain, while His13 and His14 (black) to the other one.

apical imidazole (-1.36 kcal/mol) is in the range of nonbonded interactions and small compared with equatorial imidazole (-14.91 kcal/mol). Therefore, in classical FF simulations, these weak

interactions are reasonably treated as nonbonded interactions. Only four equatorial bonds need to be treated as fixed coordination bonds. This model is identical to coordination type I of the $A\beta-Cu(II)$ complex.

Structures for Parametrization. To obtain FF parameters, optimized structures were truncated and capped with acetyl (ACE) and *N*-methylamide (NME) groups keeping only important residues that directly coordinate to copper (Asp1, His6, and His13). The choice of residues His13 or His14 as equatorial bond does not matter in term of parametrization because both of them are histidine. A truncated model built for parametrization (Figure 14) was further optimized with an unrestricted hybrid density functional method (UB3LYP) in SMD implicit solvent. In all calculations, C, N, O, and H atoms are treated with the 6-31G(d) basis set, while SDD basis set is used to treat the copper atom.

Parameters for Bonded $A\beta-Cu(II)$ Interactions. In the Amber FF, the bonded interactions including bond-stretching, bending and torsional terms are described by the first three terms in eq S1 in SI. The contribution of the torsional interaction was ignored. Thus, one has to compute the force constants (K_{ij} and K_{ijk}) and equilibrium distances (r_{ij}^{eq}) and bending angles (θ_{ijk}^{eq}) using the optimized structure (Figure 14). Single-point calculations with this structure were carried out to obtain the Hessian matrix and electrostatic potentials. FF parameters for the bond-stretching and bending interactions involving Cu(II) were extracted from the Hessian matrix using the method (Q.V.V. and M.S.L., SI) that is an improved version of the Seminario's approach.[32] Details of this method are given in SI file. FF parameters describing the bond-stretching and bending are listed in Tables 5 and 6, respectively.

van der Waals Parameters and Atomic Partial Charges. Because the copper atom is buried by four coordinated ligands, the van der Waals (vdW) interaction of the copper atom is small compared with the electrostatic one, and it is reasonable to adopt the vdW parameters of Cu(II) from Comba and Remenyi.[75] Then the vdW radius $\sigma = 1.2$ Å, the depth of the Lennard-Jones potential well $\epsilon = 0.05$ kcal/mol, and Cu(II) mass is 63.55. Using these parameters, one can obtain A_{ij} and B_{ij} in the expression for vdW term (eq S3, S4, and S5 in SI).

Single point calculations with the optimized structure at same level and basis set mentioned above were performed for estimating partial charges of copper and atoms of Asp1, His6, and His13 residues by the restrained electrostatic potential (RESP) method[76] (Table 7). Charges of atoms of capped ACE and NME residues are taken from Amber99SB force field.

All FF parameters not reported in Tables 5−7 were from the AMBER force field 99SB.[77]

MD Simulations. In order to investigate the impact of copper binding on the structure of $A\beta_{42}$ monomers and dimers, we built complexes of Cu(II) bound to a single $A\beta_{42}$ chain (monomers) and to two $A\beta_{42}$ chains (dimers), according to the following procedure. All the complexes had the initial coordinates displayed in Figure 12 concerning Cu and its ligand residues. Therefore, the Cu atom was set to coordinate to atom N and O of Asp1, atom Nδ of His6, and atom Nϵ of residue His13 for both Cu(II) + monomer and Cu(II) + dimer complexes. The coordinates of the other residues were set starting from standard geometrical parameters for bonds and angles and according to random dihedral angles for those residues not affected by Cu-binding constraints. The two different $A\beta_{42}$ chains in dimers were oriented randomly, at a distance chosen to have a mangeable simulation cell. The assemblies were centered in truncated-octahedral simulation cells with periodic boundary conditions. The box sizes and number of water molecules required by solvation are given in Table S1 in Supporting Information (SI). Note that box sizes were chosen large enough to avoid artifacts that may be caused by periodic boundary conditions. Sodium counterions (Na$^+$) were added to neutralize the system.

The Amber 14 package[78,79] was used for MD simulation with the AMBER force field 99SB[77] and water model TIP3P,[80] which is the best partner for this force field.[81,82] Equations of motion were integrated using a leapfrog algorithm[83] with a time step of 2 fs. The SHAKE algorithm[84] was used to constrain the length of all bonds related to hydrogen atoms. Temperature was controlled by Langevin thermo-
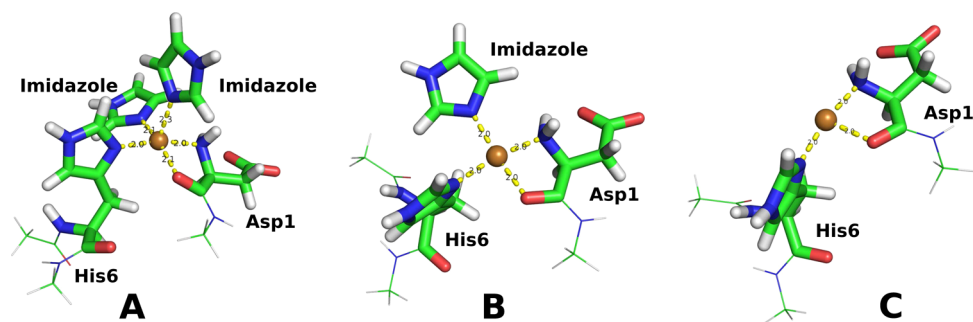
Figure 13. (A) Complex (Cu + Asp1 + His6 + 2 × imidazole). (B) Complex (Cu + Asp1 + His6 + 1 × imidazole). (C) Complex (Cu + Asp1 + His6).
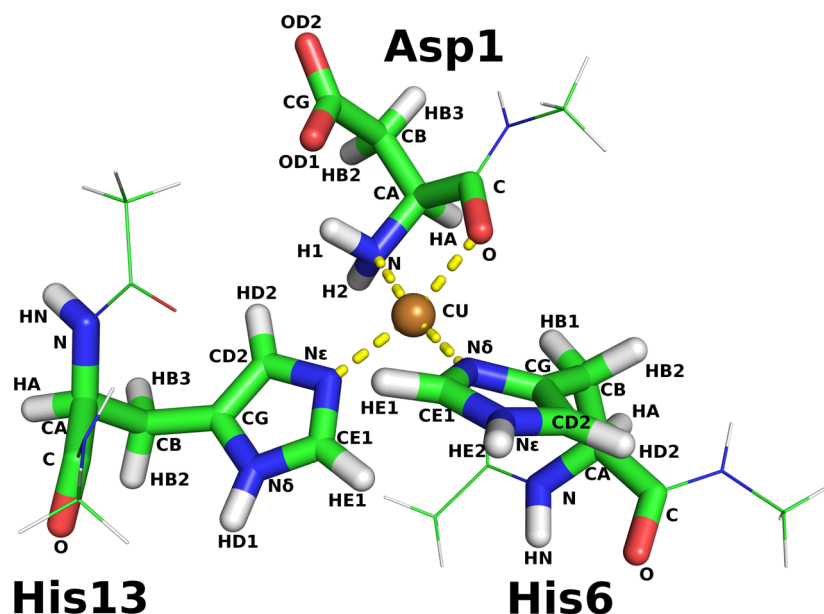

Figure 14. Final structure for FF parametrization.

Table 5. Parameters for Force Constants and Equilibrium Distances in the Bond-Stretching Interaction

bond	force constant (kcal/(mol·Å²))	R_e (Å)
Cu−N	75.272	2.017
Cu−O	50.123	2.034
Cu−Nδ	70.735	2.023
Cu−Nϵ	61.695	2.036

stat[85] with collision frequency of 2 ps⁻¹. The vdW forces were calculated with a cutoff of 1.4 nm, while 1.0 nm was used as cutoff for real-space electrostatics. No switching functions were used, and the particle mesh Ewald method[86] was employed to treat the long-range electrostatic interactions.

Measures Used in Data Analysis. The number of contacts is defined as the count of the usual distance-based step-like variable:

$$CN_2 = \sum_{i,j} s_{i,j}$$

$$s_{i,j} = 1 \quad \text{if} \quad r_{i,j} \leq 0$$

$$s_{i,j} = 0 \quad \text{if} \quad r_{i,j} > 0$$

$$r_{i,j} = |\mathbf{r}_i - \mathbf{r}_j| - d_0 \tag{3}$$

with i and j running over different sets of atom pairs and each term of the pair contained in a different portion of the system. When the two sets of atoms identify, respectively, atoms belonging to positively charged groups (Nζ in Lys and Nη in Arg) and negatively charged

Table 6. Parameters for Force Constants and Equilibrium Angles in the Bending Interaction

angle	force constant (kcal/(mol·rad²))	θ_e (deg)
N−Cu−O	35.879	81.162
N−Cu−Nδ	40.740	171.481
N−Cu−Nϵ	48.629	92.629
O−Cu−Nδ	29.769	90.411
O−Cu−Nϵ	24.734	165.202
Nδ−Cu−Nϵ	43.058	95.858
Cu−N−H1	29.605	109.209
Cu−N−H2	29.605	109.209
Cu−N−Cα	64.073	113.108
Cu−O−C	44.852	115.088
Cu−Nδ−Cγ	77.689	126.322
Cu−Nδ-Cϵ1	73.394	125.770
Cu−Nϵ−Cϵ1	68.258	127.566
Cu−Nϵ−Cδ2	71.641	125.770

groups (Cγ in Asp and Cδ in Glu), we address the contact as a salt bridge. The number of such contacts is indicated as SB, and the d_0 parameter is chosen as 4 Å. With use of eq 3, an interchain contact (ICC) is formed if the distance between centers of mass of two residues belonging to two different chains is less than d_0 = 6.5 Å. This threshold is consistent with the value of 4.5 Å used as threshold for minimal interatomic distance by statistical analysis[87] incremented of the average

Table 7. Atomic Partial Charges of Copper, Asp1, His6, and His13

Cu		Asp1		His6		His13	
atom name	charge	atom name	charge	atom name	charge	atom name	charge
Cu	0.591	N	−0.643	N	−0.423	N	−0.46
		H1	0.391	H	0.36	H	0.4
		H2	0.391	$C\alpha$	−0.532	$C\alpha$	−0.308
		$C\alpha$	−0.081	$H\alpha$	0.251	$H\alpha$	0.187
		$H\alpha$	0.1	$C\beta$	0.008	$C\beta$	−0.074
		$C\beta$	−0.389	$H\beta2$	0.118	$H\beta2$	0.11
		$H\beta2$	0.161	$H\beta3$	0.118	$H\beta3$	0.11
		$H\beta3$	0.161	$C\gamma$	−0.121	$C\gamma$	0.056
		$C\gamma$	0.756	$N\delta$	0.156	$N\delta$	−0.151
		$O\delta1$	−0.772	$C\epsilon1$	−0.158	$H\delta1$	0.35
		$O\delta2$	−0.772	$H\epsilon1$	0.218	$C\epsilon1$	0.061
		C	1.041	$N\epsilon$	−0.119	$H\epsilon1$	0.167
		O	−0.739	$H\epsilon2$	0.374	$N\epsilon$	−0.34
				$C\delta2$	−0.175	$C\delta2$	−0.126
				$H\delta2$	0.206	$H\delta2$	0.179
				C	0.958	C	0.789
				O	−0.706	O	−0.679

van der Waals radius of amino acids,[88] the latter estimated as approximately 2 Å.

As for the identification of preorganized binding sites for Cu, we use a d_0 parameter of 3 Å, this being the distance that is able to capture the first-coordination sphere of Cu when this latter is bound to Aβ. Moreover, the equation above can be extended to count the ligand atoms within clusters. The sum over a further index k running over a third set of candidate ligand atoms can be used, once the pairs $i-j$ are identified to lay within the d_0 distance. This three-body coordination number is indicated with CN_3.

Hydrogen bonds (HBs) are defined when the X−Y distance in X−H···Y is smaller than 3 Å and the X−H−Y angle is larger than 135°. The number of hydrogen bonds is indicated as HB.

Secondary structures of Aβ_{42} peptide were computed using the STRIDE algorithm[89,90] because in this algorithm the definition of second motifs is based not only on dihedral angles but also on HBs.

Free Energy Landscapes. The free energy surface (FES) along the two-dimensional reaction coordinates $V = (V_1, V_2)$ is given by $\Delta G(V) = -k_B T[\ln P(V) - \ln P_{max}]$, where $P(V)$ is the probability distribution computed using a histogram of MD data. P_{max} is the distribution maximum, which is subtracted to ascertain that $\Delta G = 0$ for the lowest-free-energy minimum. We used the gyration radius R_g and the number of interchain contacts as reaction coordinates for constructing the free energy landscape. We used the whole trajectories to compute P. A brief discussion about the information provided by FES within the limitations in time-length of our trajectories (microsecond) is reported in Supporting Information.

■ ASSOCIATED CONTENT

Ⓢ Supporting Information

The Supporting Information is available free of charge on the ACS Publications website at DOI: 10.1021/acschemneuro.6b00109.

> Derivation of force field parameters compatible with the Amber force field; details of MD simulations for all studied systems; time dependence of RMSD for all MD runs for dimers; brief discussion about convergence of time-evolution of collective variables and FES (PDF)
> Coordinates from trajectory 6 used as initial points for QM optimizations (PDB)
> Coordinates from trajectory 16 used as initial points for QM optimizations (PDB)
> Amber 14 frcmod file content used to setup the MD simulations performed with this code (TXT)
> Amber 14 lib file content used to setup the MD simulations performed with this code (TXT)

■ AUTHOR INFORMATION

Corresponding Authors

*Mai Suan Li. E-mail: masli@ifpan.edu.pl. Phone: +48 22 843 66 01.

*Giovanni La Penna. E-mail: glapenna@iccom.cnr.it. Phone: +39 055 710571.

Author Contributions

P.D.Q.H. and Q.V.V. contributed equally to the work. M.S.L. and GLP conceived the experiments. P.D.Q.H. and Q.V.V. conducted the experiments. Q.V.V., P.D.Q.H., M.S.L., and G.L.P. analyzed the results. M.S.L., Q.V.V., G.L.P., and P.D.Q.H. wrote the paper. All authors reviewed the manuscript.

■ REFERENCES

(1) Wilson, R. S., Segawa, E., Boyle, P. A., Anagnos, S. E., Hizel, L. P., and Bennett, D. A. (2012) The natural history of cognitive decline in Alzheimer's disease. *Psychol. Aging* 27, 1008−1017.

(2) Hardy, J., and Selkoe, D. J. (2002) The amyloid hypothesis of Alzheimer's disease: progress and problems on the road to therapeutics. *Science* 297, 353−356.

(3) Alonso, A., Zaidi, T., Novak, M., Grundke-Iqbal, I., and Iqbal, K. (2001) Hyperphosphorylation induces self-assembly of tau into tangles of paired helical filaments/straight filaments. *Proc. Natl. Acad. Sci. U. S. A.* 98, 6923−6928.

(4) Aguzzi, A., and O'Connor, T. (2010) Protein aggregation diseases: pathogenicity and therapeutic perspectives. *Nat. Rev. Drug Discovery* 9, 237−248.

(5) Chiang, K., and Koo, E. H. (2014) Emerging therapeutics for Alzheimer's disease. *Annu. Rev. Pharmacol. Toxicol.* 54, 381−405.

(6) Luhrs, T., Ritter, C., Adrian, M., Riek-Loher, D., Bohrmann, B., Dobeli, H., Schubert, D., and Riek, R. (2005) 3D structure of Alzheimer's amyloid-beta(1−42) fibrils. *Proc. Natl. Acad. Sci. U. S. A.* 102, 17342−17347.

(7) Petkova, A. T., Ishii, Y., Balbach, J. J., Antzutkin, O. N., Leapman, R. D., Delaglio, F., and Tycko, R. (2002) A structural model for Alzheimer's beta -amyloid fibrils based on experimental constraints from solid state NMR. *Proc. Natl. Acad. Sci. U. S. A.* 99, 16742−16747.

(8) Lesne, S., Koh, M. T., Kotilinek, L., Kayed, R., Glabe, C. G., Yang, A., Gallagher, M., and Ashe, K. H. (2006) A specific amyloid-beta protein assembly in the brain impairs memory. *Nature* 440, 352−357.

(9) Lovell, M., Robertson, J., Teesdale, W., Campbell, J., and Markesbery, W. (1998) Copper, iron and zinc in Alzheimer's disease senile plaques. *J. Neurol. Sci.* 158, 47−52.

(10) Maynard, C. J., Bush, A. I., Masters, C. L., Cappai, R., and Li, Q. X. (2005) Metals and amyloid-beta in Alzheimer's disease. *Int. J. Exp. Pathol.* 86, 147−159.

(11) Savelieff, M. G., Lee, S., Liu, Y., and Lim, M. H. (2013) Untangling amyloid-beta, tau, and metals in Alzheimer's disease. *ACS Chem. Biol. 8*, 856−865.

(12) Smith, D. G., Cappai, R., and Barnham, K. J. (2007) The redox chemistry of the Alzheimer's disease amyloid beta peptide. *Biochim. Biophys. Acta, Biomembr. 1768*, 1976−1990.

(13) Faller, P., Hureau, C., and Berthoumieu, O. (2013) Role of metal ions in the self-assembly of the Alzheimer's amyloid-beta peptide. *Inorg. Chem. 52*, 12193−12206.

(14) Drew, S. C., Masters, C. L., and Barnham, K. J. (2009) Alanine-2 Carbonyl Is an Oxygen Ligand in Cu2+ Coordination of Alzheimer's Disease Amyloid-β Peptide: Relevance to N-Terminally Truncated Forms. *J. Am. Chem. Soc. 131*, 8760−8761.

(15) Dorlet, P., Gambarelli, S., Faller, P., and Hureau, C. (2009) Pulse EPR Spectroscopy Reveals the Coordination Sphere of Copper(II) Ions in the 1−16 Amyloid-β Peptide: A Key Role of the First Two N-Terminus Residues. *Angew. Chem., Int. Ed. 48*, 9273−9276.

(16) Pedersen, J. T., Østergaard, J., Rozlosnik, N., Gammelgaard, B., and Heegaard, N. H. H. (2011) Cu(II) Mediates Kinetically Distinct, Non-amyloidogenic Aggregation of Amyloid-β Peptide. *J. Biol. Chem. 286*, 26952−26963.

(17) Innocenti, M., Salvietti, E., Guidotti, M., Casini, A., Bellandi, S., Foresti, M. L., Gabbiani, C., Pozzi, A., Zatta, P., and Messori, L. (2010) Trace Copper(II) or Zinc(II) Ions Drastically Modify the Aggregation Behavior of Amyloid-β(1−42): An AFM Study. *J. Alzheimers Dis. 19*, 1323−1329.

(18) Nasica-Labouze, J., et al. (2015) Amyloid beta Protein and Alzheimer's Disease: When Computer Simulations Complement Experimental Studies. *Chem. Rev. 115*, 3518−3563.

(19) Li, W., Zhang, J., Su, Y., Wang, J., Qin, M., and Wang, W. (2007) Effects of zinc binding on the conformational distribution of the amyloid-beta peptide based on molecular dynamics simulations. *J. Phys. Chem. B 111*, 13814−13821.

(20) Xu, L., Shan, S., Chen, Y., Wang, X., Nussinov, R., and Ma, B. (2015) Coupling of Zinc-Binding and Secondary Structure in Nonfibrillar A beta 40 Peptide Oligomerization. *J. Chem. Inf. Model. 55*, 1218−1230.

(21) Miller, Y., Ma, B., and Nussinov, R. (2010) Zinc ions promote Alzheimer A beta aggregation via population shift of polymorphic states. *Proc. Natl. Acad. Sci. U. S. A. 107*, 9490−9495.

(22) Xu, L., Wang, X., Shan, S., and Wang, X. (2013) Characterization of the polymorphic states of copper(II)-bound Aβ(1−16) peptides by computational simulations. *J. Comput. Chem. 34*, 2524−2536.

(23) Raffa, D. F., and Rauk, A. (2007) Molecular dynamics study of the beta amyloid peptide of Alzheimer's disease and its divalent copper complexes. *J. Phys. Chem. B 111*, 3789−3799.

(24) Kozmon, S., and Tvaroska, I. (2015) Molecular dynamic studies of amyloid-beta interactions with curcumin and Cu2+ ions. *Chem. Pap. 69*, 1262−1276.

(25) Raffa, D., Gomez-Balderas, R., Brunelle, P., Rickard, G., and Rauk, A. (2005) Ab initio model studies of copper binding to peptides containing a His-His sequence: relevance to the beta-amyloid peptide of Alzheimer's disease. *JBIC, J. Biol. Inorg. Chem. 10*, 887−902.

(26) Faller, P., Hureau, C., and La Penna, G. (2014) Metal Ions and Intrinsically Disordered Proteins and Peptides: From Cu/Zn Amyloid-β to General Principles. *Acc. Chem. Res. 47*, 2252−2259.

(27) Furlan, S., Faller, P., Hureau, C., and La Penna, G. (2012) Modeling Cu-Aβ(1−16) Complex at Different pH: Towards a Molecular Mechanism for Cu Reduction. *J. Phys. Chem. B 116*, 11899−11910.

(28) La Penna, G., Hureau, C., Andreussi, O., and Faller, P. (2013) Identifying, by First-Principles Simulations, Cu[Amyloid-β] Species Making Fenton-Type Reactions in Alzheimers Disease. *J. Phys. Chem. B 117*, 16455−16467.

(29) Parthasarathy, S., Long, F., Miller, Y., Xiao, Y., McElheny, D., Thurber, K., Ma, B., Nussinov, R., and Ishii, Y. (2011) Molecular-level examination of Cu2+ binding structure for amyloid fibrils of 40-residue Alzheimer's disease by solid-state NMR spectroscopy. *J. Am. Chem. Soc. 133*, 3390−3400.

(30) Weiner, S. J., Kollman, P. A., Case, D. A., Singh, U. C., Ghio, C., Alagona, G., Profeta, S., and Weiner, P. (1984) A new force field for molecular mechanical simulation of nucleic acids and proteins. *J. Am. Chem. Soc. 106*, 765−784.

(31) Cornell, W. D., Cieplak, P., Bayly, C. I., Gould, I. R., Merz, K. M., Ferguson, D. M., Spellmeyer, D. C., Fox, T., Caldwell, J. W., and Kollman, P. A. (1995) A Second Generation Force Field for the Simulation of Proteins, Nucleic Acids, and Organic Molecules. *J. Am. Chem. Soc. 117*, 5179−5197.

(32) Seminario, J. M. (1996) Calculation of intramolecular force fields from second-derivative tensors. *Int. J. Quantum Chem. 60*, 1271−1277.

(33) Furlan, S., Hureau, C., Faller, P., and La Penna, G. (2012) Modeling copper binding to the amyloid-beta peptide at different pH: toward a molecular mechanism for Cu reduction. *J. Phys. Chem. B 116*, 11899−11910.

(34) Straub, J. E., and Thirumalai, D. (2011) *Annu. Rev. Phys. Chem. 62*, 437−463.

(35) Galindo-Murillo, R., Roe, D. R., and Cheatham, T. E., III (2015) Convergence and Reproducibility in Molecular Dynamics Simulations of the DNA Duplex d(GCACGAACGAACGAACGC). *Biochim. Biophys. Acta, Gen. Subj. 1850*, 1041−1058.

(36) Sawle, L., and Ghosh, K. (2016) Convergence of Molecular Dynamics Simulation of Protein Native States: Feasibility vs Self-Consistency Dilemma. *J. Chem. Theory Comput. 12*, 861−869.

(37) Kabsch, W. (1976) A Solution for the Best Rotation to Relate Two Sets of Vectors. *Acta Crystallogr., Sect. A: Cryst. Phys., Diffr., Theor. Gen. Crystallogr. A32*, 922−923.

(38) Nag, S., Sarkar, B., Bandyopadhyay, A., Sahoo, B., Sreenivasan, V. K. A., Kombrabail, M., Muralidharan, C., and Maiti, S. (2011) Nature of the Amyloid-β Monomer and the Monomer-Oligomer Equilibrium. *J. Biol. Chem. 286*, 13827−13833.

(39) Sitkiewicz, E., Kłoniecki, M., Poznański, J., Bal, W., and Dadlez, M. (2014) Factors Influencing Compact-Extended Structure Equilibrium in Oligomers of Aβ1−40 Peptide - An Ion Mobility Mass Spectrometry Study. *J. Mol. Biol. 426*, 2871−2885.

(40) Kollman, P., Massova, I., Reyes, C., Kuhn, B., Huo, S., Chong, L., Lee, M., Lee, T., Duan, Y., Wang, W., Donini, O., Cieplak, P., Srinivasan, J., Case, D., and Cheatham, T. (2000) Calculating structures and free energies of complex molecules: Combining molecular mechanics and continuum models. *Acc. Chem. Res. 33*, 889−897.

(41) Sharp, K., and Honig, B. (1990) Electrostatic interactions in macromolecules - Theory and application. *Annu. Rev. Biophys. Biophys. Chem. 19*, 301−332.

(42) Sitkoff, D., Sharp, K., and Honig, B. (1994) Accurate calculation of hydration free-energies using macroscopic solvent modeles. *J. Phys. Chem. 98*, 1978−1988.

(43) Li, M. S., Co, N. T., Reddy, G., Hu, C.-K., Straub, J. E., and Thirumalai, D. (2010) Factors Governing Fibrillogenesis of Polypeptide Chains Revealed by Lattice Models. *Phys. Rev. Lett. 105*, 218101.

(44) Chiti, F., Stefani, M., Taddei, N., Ramponi, G., and Dobson, C. (2003) Rationalization of the effects of mutations on peptide and protein aggregation rates. *Nature 424*, 805−808.

(45) Teplow, D. B., Lazo, N. D., Bitan, G., Bernstein, S., Wyttenbach, T., Bowers, M. T., Baumketner, A., Shea, J.-E., Urbanc, B., Cruz, L., Borreguero, J., and Stanley, H. E. (2006) Elucidating amyloid beta-protein folding and assembly: A multidisciplinary approach. *Acc. Chem. Res. 39*, 635−645.

(46) Sciarretta, K. L., Gordon, D. J., Petkova, A. T., Tycko, R., and Meredith, S. C. (2005) A beta 40-Lactam(D23/K28) Models a Conformation Highly Favorable for Nucleation of Amyloid. *Biochemistry 44*, 6003−6014.

(47) Reddy, G., Straub, J. E., and Thirumalai, D. (2009) Influence of Preformed Asp23-Lys28 Salt Bridge on the Conformational Fluctuations of Monomers and Dimers of A Beta Peptides with Implications for Rates of Fibril Formation. *J. Phys. Chem. B 113*, 1162−1172.

(48) Viet, M. H., Nguyen, P. H., Ngo, S. T., Li, M. S., and Derreumaux, P. (2013) Effect of the Tottori Familial Disease Mutation (D7N) on the Monomers and Dimers of Aβ40 and Aβ42. *ACS Chem. Neurosci. 4*, 1446−1457.

(49) Viet, M. H., Nguyen, P. H., Derreumaux, P., and Li, M. S. (2014) Effect of the English Familial Disease Mutation (H6R) on the Monomers and Dimers of Aβ40 and Aβ42. *ACS Chem. Neurosci. 5*, 646.

(50) Rosenman, D. J., Connors, C., Chen, W., Wang, C., and Garcia, A. E. (2013) Aβ Monomers Transiently Sample Oligomer and Fibril-like Configurations: Ensemble Characterization Using a Combined MD/NMR Approach. *J. Mol. Biol. 425*, 3338−3359.

(51) Ball, K. A., Phillips, A. H., Wemmer, D. E., and Head-Gordon, T. (2013) Differences in β-strand Populations of Monomeric Aβ40 and Aβ42. *Biophys. J. 104*, 2714−2724.

(52) Sgourakis, N. G., Yan, Y. L., McCallum, S. A., Wang, C. Y., and Garcia, A. E. (2007) The Alzheimer's Peptides A Beta 40 and 42 Adopt Distinct Conformations in Water: A Combined MD/NMR Study. *J. Mol. Biol. 368*, 1448−1457.

(53) Viet, M. H., and Li, M. S. (2012) Amyloid Peptide Aβ$_{40}$ Inhibits Aggregation of Aβ$_{42}$: Evidence from Molecular Dynamics Simulations. *J. Chem. Phys. 136*, 245105.

(54) Velez-Vega, C., and Escobedo, F. A. (2011) Characterizing the Structural Behavior of Selected A Beta-42 Monomers with Different Solubilities. *J. Phys. Chem. B 115*, 4900−4910.

(55) Cote, S., Derreumaux, P., and Mousseau, N. (2011) Distinct Morphologies for Amyloid Beta Protein Monomer: A Beta(1−40), A Beta(1−42), and A Beta(1−40)(D23N). *J. Chem. Theory Comput. 7*, 2584−2592.

(56) Sgourakis, N. G., Merced-Serrano, M., Boutsidis, C., Drineas, P., Du, Z. M., Wang, C. Y., and Garcia, A. E. (2011) Atomic-level Characterization of the Ensemble of the A Beta(1−42) Monomer in Water Using Unbiased Molecular Dynamics Simulations and Spectral Algorithms. *J. Mol. Biol. 405*, 570−583.

(57) Truong, P. M., Viet, M. H., Nguyen, P. H., Hu, C.-K., and Li, M. S. (2014) Effect of Taiwan Mutation (D7H) on Structures of Amyloid-beta Peptides: Replica Exchange Molecular Dynamics Study. *J. Phys. Chem. B 118*, 8972−8981.

(58) Yang, M., and Teplow, D. B. (2008) Amyloid β-protein Monomer Folding: Free Energy Surfaces Reveal Alloform-specific Differences. *J. Mol. Biol. 384*, 450−464.

(59) Mitternacht, S., Staneva, I., Hard, T., and Irback, A. (2010) Comparing the Folding Free-energy Landscapes of A Beta 42 Variants with Different Aggregation Properties. *Proteins: Struct., Funct., Genet. 78*, 2600−2608.

(60) Ono, K., Condron, M. M., and Teplow, D. B. (2009) Structure-neurotoxicity relationships of amyloid beta-protein oligomers. *Proc. Natl. Acad. Sci. U. S. A. 106*, 14745−14750.

(61) Huang, T., Yang, D., Plaskos, N., Go, S., Yip, C., Fraser, P., and Chakrabartty, A. (2000) Structural studies of soluble oligomers of the Alzheimer beta-amyloid peptide. *J. Mol. Biol. 297*, 73−87.

(62) Bitan, G., Vollers, S., and Teplow, D. (2003) Elucidation of primary structure elements controlling early amyloid beta-protein oligomerization. *J. Biol. Chem. 278*, 34882−34889.

(63) Urbanc, B., Betnel, M., Cruz, L., Bitan, G., and Teplow, D. B. (2010) Elucidation of Amyloid beta-Protein Oligomerization Mechanisms: Discrete Molecular Dynamics Study. *J. Am. Chem. Soc. 132*, 4266−4280.

(64) Barz, B., and Urbanc, B. (2012) Dimer Formation Enhances Structural Differences between Amyloid beta-Protein (1−40) and (1−42): An Explicit-Solvent Molecular Dynamics Study. *PLoS One 7*, e34345.

(65) Zhang, T., Zhang, J., Derreumaux, P., and Mu, Y. (2013) Molecular Mechanism of the Inhibition of EGCG on the Alzheimer A beta(1−42) Dimer. *J. Phys. Chem. B 117*, 3993−4002.

(66) Tarus, B., Straub, J. E., and Thirumalai, D. (2008) Structures and Free-Energy Landscapes of the Wild Type and Mutants of the Aβ21−30 Peptide Are Determined by an Interplay between Intrapeptide Electrostatic and Hydrophobic Interactions. *J. Mol. Biol. 379*, 815−829.

(67) Petkova, A. T., Ishii, Y., Balbach, J. J., Antzutkin, O. N., Leapman, R. D., Delaglio, F., and Tycko, R. (2002) A Structural Model for Alzheimer's β-Amyloid Fibrils Based On Experimental Constraints From Solid State NMR. *Proc. Natl. Acad. Sci. U. S. A. 99*, 16742−16747.

(68) Buchete, N.-V., and Hummer, G. (2007) Structure and Dynamics of Parallel β-Sheets, Hydrophobic Core, and Loops in Alzheimer's Aβ Fibrils. *Biophys. J. 92*, 3032−3039.

(69) Tofoleanu, F., and Buchete, N.-V. (2012) Molecular Interactions of Alzheimer's Aβ Protofilaments with Lipid Membranes. *J. Mol. Biol. 421*, 572−586.

(70) Tofoleanu, F., Brooks, B. R., and Buchete, N.-V. (2015) Modulation of Alzheimer's Aβ Protofilament-Membrane Interactions by Lipid Headgroups. *ACS Chem. Neurosci. 6*, 446−455.

(71) Lewandowska, A., Oldziej, S., Liwo, A., and Scheraga, H. A. (2010) beta-hairpin-forming peptides; models of early stages of protein folding. *Biophys. Chem. 151*, 1−9.

(72) La Penna, G., Hureau, C., and Faller, P. (2015) Learning Chemistry with Multiple First-principles Simulations. *Mol. Simul. 41*, 780−787.

(73) Marenich, A. V., Cramer, C. J., and Truhlar, D. G. (2009) Universal Solvation Model Based on Solute Electron Density and on a Continuum Model of the Solvent Defined by the Bulk Dielectric Constant and Atomic Surface Tensions. *J. Phys. Chem. B 113*, 6378−6396 PMID: 19366259..

(74) Frisch, M. J., Trucks, G. W., Schlegel, H. B., Scuseria, G. E., Robb, M. A., Cheeseman, J. R., Scalmani, G., Barone, V., Mennucci, B., Petersson, G. A., Nakatsuji, H., Caricato, M., Li, X., Hratchian, H. P., Izmaylov, A. F., Bloino, J., Zheng, G., Sonnenberg, J. L., Hada, M., Ehara, M., Toyota, K., Fukuda, R., Hasegawa, J., Ishida, M., Nakajima, T., Honda, Y., Kitao, O., Nakai, H., Vreven, T., Montgomery, J. A., Jr., Peralta, J. E., Ogliaro, F., Bearpark, M., Heyd, J. J., Brothers, E., Kudin, K. N., Staroverov, V. N., Kobayashi, R., Normand, J., Raghavachari, K., Rendell, A., Burant, J. C., Iyengar, S. S., Tomasi, J., Cossi, M., Rega, N., Millam, J. M., Klene, M., Knox, J. E., Cross, J. B., Bakken, V., Adamo, C., Jaramillo, J., Gomperts, R., Stratmann, R. E., Yazyev, O., Austin, A. J., Cammi, R., Pomelli, C., Ochterski, J. W., Martin, R. L., Morokuma, K., Zakrzewski, V. G., Voth, G. A., Salvador, P., Dannenberg, J. J., Dapprich, S., Daniels, A. D., Farkas, O., Foresman, J. B., Ortiz, J. V., Cioslowski, J., and Fox, D. J. (2009) *Gaussian 09*, revision D.01, Gaussian, Inc., Wallingford, CT.

(75) Comba, P., and Remenyi, R. (2002) A new molecular mechanics force field for the oxidized form of blue copper proteins. *J. Comput. Chem. 23*, 697−705.

(76) Cornell, W. D., Cieplak, P., Bayly, C. I., and Kollmann, P. A. (1993) Application of RESP charges to calculate conformational energies, hydrogen bond energies, and free energies of solvation. *J. Am. Chem. Soc. 115*, 9620−9631.

(77) Hornak, V., Abel, R., Okur, A., Strockbine, B., Roitberg, A., and Simmerling, C. (2006) Comparison of Multiple Amber Force Fields and Development of Improved Protein Backbone Parameters. *Proteins: Struct., Funct., Genet. 65*, 712−725.

(78) Pearlman, D. A., Case, D. A., Caldwell, J. W., Ross, W. S., III, Cheatham, T. E., DeBolt, S., Ferguson, D., Seibel, G., and Kollman, P. (1995) AMBER, a package of computer programs for applying molecular mechanics, normal mode analysis, molecular dynamics and free energy calculations to simulate the structural and energetic properties of molecules. *Comput. Phys. Commun. 91*, 1−41.

(79) Case, D. A., Cheatham, T. E., Darden, T., Gohlke, H., Luo, R., Merz, K. M., Onufriev, A., Simmerling, C., Wang, B., and Woods, R. J. (2005) The Amber biomolecular simulation programs. *J. Comput. Chem. 26*, 1668−1688.

(80) Jorgensen, W. L., Chandrasekhar, J., Madura, J. D., Impey, R. W., and Klein, M. L. (1983) Comparison of simple potential functions for simulating liquid water. *J. Chem. Phys. 79*, 926−935.

(81) van Gunsteren, W. F., Billeter, S. R., Eising, A. A., Hunenberger, P. H., Kruger, P., Mark, A. E., Scott, W. R. P., and Tironi, I. G. (1996) *Biomolecular Simulation: The GROMOS96 Manual and User Guide*; Vdf Hochschulverlag AG an der ETH Zurich, Zurich.

(82) Nguyen, T. T., Viet, M. H., and Li, M. S. (2014) Effects of water models on binding affin- ity: Evidence from all-atom simulation of binding of tami u to A/H5N1 neu- raminidase. *Sci. World J. 2014*, 36084.

(83) Hockney, R., Goel, S., and Eastwood, J. (1974) Quiet high-resolution computer models of a plasma. *J. Comput. Phys. 14*, 148−158.

(84) Ryckaert, J.-P., Ciccotti, G., and Berendsen, H. J. (1977) Numerical integration of the cartesian equations of motion of a system with constraints: molecular dynamics of n-alkanes. *J. Comput. Phys. 23*, 327−341.

(85) Wu, X. W., and Brooks, B. R. (2003) Self-guided langevin dynamics simulation method. *Chem. Phys. Lett. 381*, 512−518.

(86) Darden, T., York, D., and Pedersen, L. (1993) Particle mesh Ewald: An Nlog(N) method for Ewald sums in large systems. *J. Chem. Phys. 98*, 10089−10092.

(87) Bastolla, U., Porto, M., Roman, H. E., and Vendruscolo, M. (2005) Principal Eigenvector of Contact Matrices and Hydrophobicity Profiles in Proteins. *Proteins: Struct., Funct., Genet. 58*, 22−30.

(88) Darby, N. J., and Creighton, T. E. (1993) *Protein Structure*, Oxford University Press, New York.

(89) Frishman, D., and Argos, P. (1995) Knowledge-Based Protein Secondary Structure Assignment. *Proteins: Struct., Funct., Genet. 23*, 566−579.

(90) Heinig, M., and Frishman, D. (2004) STRIDE: a Web Server for Secondary Structure Assignment from Known Atomic Coordinates of Proteins. *Nucleic Acids Res. 32*, W500−2.